

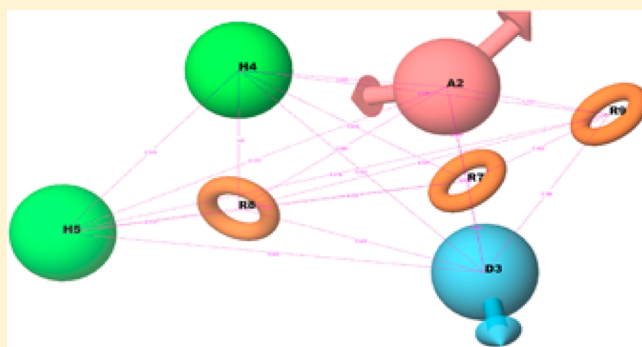
Computational Prediction of a Putative Binding Site on Drp1: Implications for Antiparkinsonian Therapy

Hanumanthappa Pradeep and G. Krishnamurthy Rajanikant*

School of Biotechnology, National Institute of Technology Calicut, Calicut 673601, Kerala, India

Supporting Information

ABSTRACT: Parkinson's disease is the second most common neurodegenerative disorder, for which no cure or disease-modifying therapies exist. It is evident that mechanisms impairing mitochondrial dynamics will damage cell signaling pathways, leading to neuronal death that manifests as Parkinson's disease. Dynamin related protein1, a highly conserved protein that catalyzes the process of mitochondrial fission, is also associated with the excessive fragmentation of mitochondria, impaired mitochondrial dynamics and cell death. Hence, Dynamin related protein1 has emerged as a key therapeutic target for diseases involving mitochondrial dysfunction. In this work, we employed a relatively novel and integrated computational strategy to identify a cryptic binding site of Dynamin related protein1 and exploited the predicted site in the rational drug designing process. This novel approach yielded three potential inhibitors, and all of them were evaluated for their neuroprotective efficacy in *C. elegans* model of Parkinson's disease.



INTRODUCTION

Parkinson's disease (PD) is the second most common neurodegenerative disorder after Alzheimer's disease and manifests as bradykinesia (slowed movement), rigidity, resting tremor, and posture instability.¹ There is currently no available treatment to either prevent or slow down the dopaminergic neuronal loss and the resulting dopamine (a neurotransmitter) decrease in the midbrain.¹ Mounting evidence demonstrates that Dynamin related protein 1 (Drp1), a master regulator of mitochondrial division, plays a critical role in the pathogenesis of Parkinson's disease.^{2–4} Drp1 is an authorized substrate of "neurotoxic factors" such as oligomerized synuclein, mutant huntingtin, and parkin, all of which have been demonstrated to accelerate its GTPase activity, leading to excessive mitochondrial fission and neuronal degeneration.^{5–7} Therefore, the Drp1 inhibition directed at optimizing mitochondrial dynamics may offer a novel therapeutic approach for the treatment of PD.

A number of small molecule inhibitors of Drp1 with the potential to emerge as neurotherapeutics have recently been identified (Dynasore and P110).^{8,9} Nonspecific Drp1 antagonists inhibit the GTP hydrolysis in a noncompetitive manner by binding to the GTPase domain.⁸ However, the GTPase domain of Drp1 is the site of GTP binding and hence the most highly conserved domain in the GTPase superfamily. Targeting the GTPase domain will affect the entire dynamin family of GTPases and would be therapeutically toxic. In this regard, identifying an alternative target site would be a potential therapeutic strategy.

Proteins in nature quite often possess allosteric binding site/s to which a ligand can bind to direct the activity of the protein. Finding and targeting sites other than the standard binding site represents a new and safer mode of targeting a protein.¹² Many strategies can be developed and have been developed to exploit the known receptor of the protein for specific drug binding. However, designing a drug for an unknown receptor is tricky and challenging. The major hurdle in such effort is the lack of the known receptor itself. Hence, developing new strategies for identifying such allosteric sites would open up new ways in formulating novel therapeutics against human diseases. Growing evidence suggest that Drp1 possesses an unexplored site targeted by a selective ligand.^{10,11} This allosteric site may not interact with any natural ligand and/or may have been only adventitiously exploited by the small molecule that binds there. Strikingly, this binding is sufficient to allosterically exert an inhibitory effect on the GTPase activity of Drp1.^{11,12} Despite this knowledge, the precise location of this unique allosteric site of Drp1 remains unexplored, which is in part due to the complex nature of Drp1 and the lack of a published structure to guide such efforts.

Here we are proposing one such strategy that is conceptualized to predict and exploit the "cryptic" allosteric site on Drp1 for the drug designing process (Figure 1). The structure-based site mapping protocol was employed to identify the potential allosteric sites on Drp1. The obtained sites were

Received: February 15, 2014

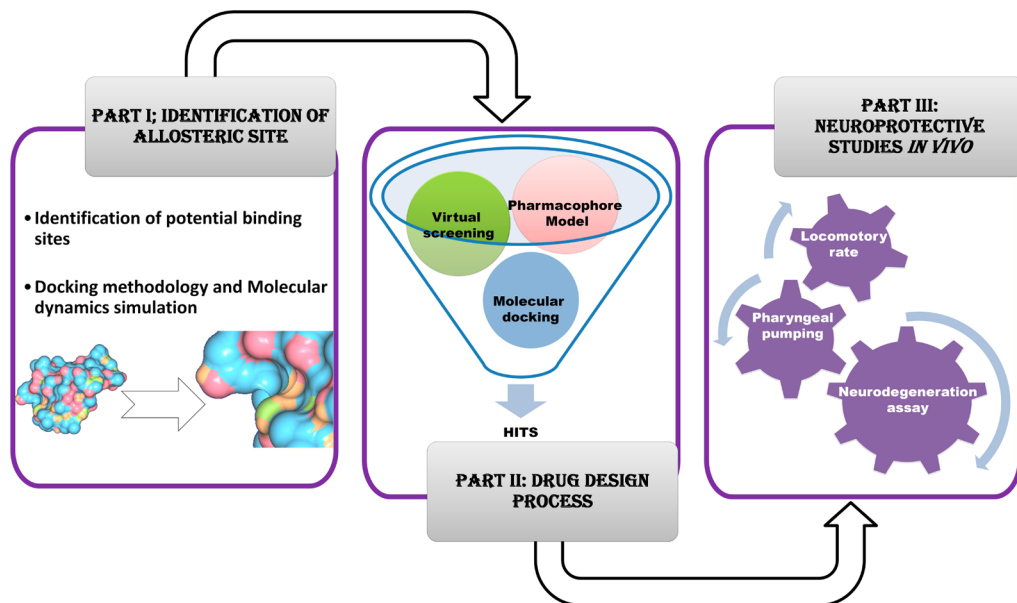


Figure 1. Workflow depicting the process of *in silico* design and *in vivo* evaluation of Drp1 inhibitors.

Table 1. Potential Binding Sites Identified in the Modeled Drp1

name	site score	size	Dscore	volume	enclosure	contact	GlideScore
Site-1	1.1	163	0.81	288	0.82	1.10	-2.6
Site-2	1.1	115	1.17	284	0.78	0.98	-7.25
Site-3	0.78	50	0.75	162	0.66	0.87	-1.7
Site-4	0.75	46	0.69	125	0.68	0.81	-3.5
Site-5	0.68	39	0.54	107	0.63	0.80	-2.8
Site-6	0.76	46	0.69	81.0	0.69	0.92	-3.2
Site-7	0.75	34	0.60	80.9	0.70	0.90	-4.5
Site-8	0.69	35	0.64	92.6	0.65	0.89	-2.4

subjected to docking based screening and validated by molecular dynamics (MD) simulation. Further, a structure-based pharmacophore model for the identified cryptic site was developed and used to perform a virtual screening of small molecule database. The identified compounds were further refined by molecular docking and were evaluated for their neuroprotective efficacy in *C. elegans* model of PD.

MATERIAL AND METHODS

Homology Model of Drp1. The primary sequence of human Drp1 (Accession Number NP_036192.2) was retrieved from NCBI. The crystal structure of Dynamin protein of *Dictyostelium discoideum* was retrieved from the PDB (ID: 1JWY)¹³ and was used as the template for homology modeling of Drp1. Dynamin showed 61% sequence identity, 82% similarity, and E-value of 3e-143. The process of sequence alignment and model building was carried out in Prime module of the Schrödinger.^{14,15} MolProbity¹⁶ and PROCHECK¹⁷ were used to assess the quality of the models.

Identification of Potential Binding Sites. SiteMap¹⁶ module of the Schrödinger was used to predict all the binding sites on the modeled Drp1. SiteMap identifies the potential binding sites and also predicts their druggability. Site score is an important property generated by SiteMap to identify the binding sites.¹⁸ Other properties computed by SiteMap module are the size of the site, the degrees of enclosure by the protein and exposure to solvent, and the tightness with which the site points interact with the receptor. Total eight binding sites (1–

8) with maximum site score, druggability score, and the volume were considered for further analysis (Table 1).

Docking Methodology. Molecular docking is a central method in computational drug design that flexibly aligns the ligand molecules into the receptor site and then estimates the tightness of the interactions.^{19,20} The docking takes all the information from a flexible protein environment and scores several possible interaction modes for different orientations.^{21,22}

All eight sites with good SiteMap scores were considered to generate Glide scoring grids for the subsequent docking calculations. To each of the identified sites, a grid box of 20 × 20 × 20 Å was assigned. Default parameters were used, and no constraints were included during grid generation. The selective inhibitor, Mdivi-1 obtained from ChemSpider, was subjected to hydrogen additions, removal of salt, ionization, and generation of low-energy ring conformations using LigPrep.^{23,24} Finally, a low-energy 3D structure of the inhibitor was employed in the docking process. Docking study was performed on Glide^{25,26} running on Windows XP. All the Glide protocols were executed using default parameters. During the docking process, the G-score was used to select the best conformation of the ligand.

Molecular Dynamics Simulation. Based on the analysis of docking results, three probable binding sites (2, 4, and 7) with good docking scores were selected to carry out the multinano-second MD simulations using the GROMACS v4.6²⁷ with GROMOS 53a5 force field.²⁸ We employed two modes of

simulation viz., [1] three separate simulations for three potential binding sites with Mdivi-1 docked to each of the receptor and [2] a combined simulation with Mdivi-1 placed 5 Å away from each potential binding site. Further, MD simulation of Drp1 without Mdivi-1 (Apo-form) was also performed to compare the changes upon the binding of Mdivi-1. PRODRG,²⁹ a force field generation tool, was used to generate topologies and parameters for ligands, which computes based on the ffpmx force field, but in a functional form that is compatible with the GROMOS force field.

Prior to the execution of MD simulation, the system underwent 10,000 steps of steepest descent minimization, followed by explicit solvation in a cubical water system. The system comprised of 37,518 TIP3P water molecules³⁰ with a salt concentration of 0.1 M NaCl. Additional 10,000 steps of steepest descent energy minimization were employed to properly allow the solvent molecules to adjust/relax around the protein. After energy minimization all the systems were equilibrated for 100 ps with NVT and NPT ensemble equilibration protocol for about 100 ps, with the protein backbone atoms restrained in order to prevent adsorption before equilibration. Extensive MD simulations were then performed for a total of 20 or 40 ns under a constant number of particles at a constant temperature of 310 K using Berendsen's method³¹ and at a constant pressure of 1 bar with a 2.0 fs time step. The linear constraint (LINCS) algorithm was applied to fix all hydrogen related bond lengths, facilitating the use of a 2 fs time step. Particle Mesh Ewald (PME)³² was employed to treat long-range electrostatic interactions. Analyses were carried out using the GROMACS analysis package and visual molecular dynamics (VMD).³³ The atomic positions were saved every 250 steps (0.5 ps), and the last 10 ns were used for the analysis.

Mutational Analysis. Further, we have analyzed the Site-2 cavity in more detail, with the aim of identifying the key residues involved in its allosteric activity. First, we examined the interaction profile of Mdivi-1 at the Site-2 and identified Leu217, Phe268, and Tyr273 as key residues that are involved with Mdivi-1 during docking. Later, in order to build the mutant structures, we made a point mutation in native Drp1 protein at L217S (leucine to serine), F268K (phenylalanine to lysine), and Y273A (tyrosine to alanine) using Maestro, and these mutated structures were subjected to multinano second MD simulation.

The mutant structures were energetically optimized by applying the GROMOS 53a5 force field available under the GROMACS. The structure of mutant Drp1 protein with Mdivi-1 bound at the Site-2 was used as starting point for MD simulations. Systems were solvated in a cubic box with TIP3P water molecules at 11 Å marginal radiiuses. All the previously employed parameters were considered for running 20 ns simulations.

Pharmacophore Generation and Virtual Screening.

The hybrid of fragment- and structure-based pharmacophore modeling approach that uses energetic analysis of docked fragments was employed to generate pharmacophore hypotheses. The predicted allosteric site, Site-2, was subjected to novel a E-pharmacophore approach to generate energy-optimized pharmacophores.³⁴ The best pharmacophore hypothesis ADHRRR was selected based on the careful observation of feature scores and alignment of fragments to the generated hypotheses. The pharmacophore model developed was employed as a structural query in screening the ZINC database.

The ZINC pharmer tool was used (<http://zincpharmer.csbi.pitt.edu>) to retrieve hits that fit the hypothesis.³⁵

Molecular Docking. All the hits with good RMSD value were enlisted and were incorporated into Maestro (Schrodinger, LLC). Hits were subjected to hydrogen additions, removal of salt, ionization, and generation of low-energy ring conformations using LigPrep. The chiralities of the original compounds were preserved. Finally, the low-energy 3D structures of all compounds were produced. The docking grid was generated using site-2 region of the modeled structure and subsequently employed in the docking process. The docking protocols were implemented as explained earlier in the "Docking methodology" section. The G-score was used to select the best conformation for each ligand.

Worm Strains and Maintenance. *Ceutorhynchus elegans* model of Parkinson's disease was used to evaluate the neuroprotective efficacy of Drp1 inhibitors *in vivo*.³⁶ Mutant strains used were Pdat-1::GFP animals (strain BZ555), Pdat-1::α-syn (strain UA44), obtained from the Caldwell Laboratory, University of Alabama, USA. We employed wildtype (N2) strain as the control group. Nematodes were grown in noncrowded conditions at 20 °C; *E. coli* strain OP50 was used as the food source. The plates containing worm-laid eggs were washed with M9 buffer and treated using a standard age synchronizing protocol.³⁷

Small Molecule Exposure. The worms that hatched 48 h after synchronization were transferred to 24-well microtiter plate for pretreatment. The test compounds (ZINC09087302, ZINC05460903, and ZINC13204615, represented as DI1, 2, and 3, respectively) were diluted in DMSO and added to the wells at final concentrations of 50 and 100 μM. A total of 100 worms were added to each well, with 2 wells for each group.

Locomotory Rate and Pharyngeal Pumping Assays. After 10 days of constant drug exposure, worms were employed in the assay process. Locomotory behavior was analyzed in wildtype (N2) and mutant (UA44) worms using visual (individual and group assays) methods. Worms were synchronously grown to early adult stage and placed in individual wells of a 24-well microtiter plate, containing 500 μL of M9 with or without drug. After a 10 min exposure period to M9, thrashes were counted at 21 °C for 30 s. A single thrash was defined as a complete change in the direction of bending at the mid body. Manual counting was performed independently by two trained experimenters. Each experiment was repeated three times.

Feeding rates were measured following the previous protocol.³⁸ Briefly, pharyngeal bulb contractions were measured at room temperature. Worms were synchronously grown to L1 stage and placed in individual wells of a 24-well microtiter plate containing 500 μL of M9 with or without drug. The number of contractions was counted over 20 s in triplicate, and the average was used for statistical analyses. For each condition, ten animals were used. Each experiment was repeated three times.

Neurodegeneration Assay. The worm embryos were grown under constant exposure to test compounds, and a total of 5–10 worms were scored for neurodegeneration after 10 days of drug exposure. The Pdat-1::GFP animals (strains BZ555) and Pdat-1::α-syn (strain UA44) animals were used for the analyses in all the experiments. For observation under microscope, worms were immobilized with a small aliquot of 100 mM sodium azide on a microscope slide. CX 31 (Olympus) epifluorescence microscope equipped with an Endow GFP HYQ filter cube was used to visualize the

fluorescence. A wide zoom camera (Olympus) was used to acquire images. Worms were considered as normal when all six anterior dopaminergic neurons (two ADE (anterior deirid) and four CEP (cephalic)) were intact, and no visible signs of degeneration were observed. If a worm displayed a neuron with any degenerative change (missing neuronal processes, rounding or cell body loss, or blebbing process), then it was scored as exhibiting a degenerative phenotype.

Statistical Analysis. Data were presented as mean \pm SEM. Statistical significance of differences between the results was analyzed using the two ways ANOVA followed by the Tukey–Kramer post hoc test for multiple comparisons. A *p*-value <0.05 was considered significant.

RESULTS AND DISCUSSION

Homology Model of the Drp1. We have used the B chain of the Dynamin (PDB ID: 1JWY) as the template for homology modeling of Drp1. Dynamin has a high degree of homology with Drp1. It was used as a template with identity of 61% with atomic resolution of its X-ray crystal structure at 2.3 Å and R value being 0.203. The Alignment Score and the Root Mean Square Deviation (RMSD) value between the template and predicted loop model were found to be 0.00808 and 0.45, respectively, which are often indicative of a good model (Figure 2). The Ramachandran plot indicated the region of possible angle formations by Φ (phi) and ψ (psi) angles (Supplementary 1).



Figure 2. Best homology model of the functional domain of the Drp1.

Prediction of Probable Binding Sites. A map signature was generated for all the possible binding sites on the modeled protein structure. SiteMap was used to locate potential binding hot spots. SiteMap is an energetic grid based method, which correlates pocket druggability with propensity to the binding of small molecules. Finally, the Sitemap identified ten potential binding sites in the modeled domain. We selected the eight putative site exhibiting the maximum volume and druggability score (D-Score) (Table 1). Further, the Sitemap revealed the following features, namely H-bond acceptor, H-bond donor, hydrophilic, hydrophobic, and metal binding surfaces.

Docking Mode Analysis. In our approach, molecular docking occupies a very important position, so we have used molecular docking as a primary screening tool and it assisted not only with screening out almost all undesirable sites but also with rationalizing the binding mode of Mdivi-1 on Site-2. The performance of molecular docking was evaluated by comparing the docked binding poses of Mdivi-1 in each receptor grids. The binding efficiency of the highest scoring interactions from docking studies and the Glide scoring function value (G-score) (ranging between -1.78 to -7.29) are shown in Table 1. More negative G-score value indicates better interaction of the inhibitor with the target site. A comparison of different docking poses suggests that the three putative sites showed good binding interaction against Mdivi-1 with more negative G-Score values (viz., Site-2, Site-4, and Site-4).

The interaction pattern obtained for Site-2 suggests that the 2-sulfanyl-4(3H)-quinazolinone scaffold of Mdivi-1 is well placed in the cavity, while the dichloro-methoxyphenyl moiety peeks out from the outer surface of the receptor (Figure 3a). The hydroxyl group of Tyr273 forms a H-bond with the NH group at 2-position of the quinazolinone moiety. In addition, another weak H-bonding interaction between the NH group of Ala226 and the oxygen at 4-position also contributes to the affinity of Mdivi-1. Further, residues Leu217, Val245, Phe268, Leu269, Lys271, Ala272, and Tyr273 constitute the hydrophobic binding pocket, which accommodates the whole quinazolinone moiety of the ligand. Figure 3b depicts the docking mode of Mdivi-1 in the Site-4, from which we can deduce that 2-sulfanyl-4(3H)-quinazolinone scaffold is encased in the hydrophilic cavity, while the dichloromethoxyphenyl moiety is located on the surface of the receptor. Further, visual analysis shows that there is a strong H-bond interaction between the carboxyl group of Ser159 and the NH group at the 2-position of the quinazolinone moiety. In addition, another H-bonding interaction is also seen between the carboxyl group of Ser158 and the NH group. Binding analysis of the Site-7 Mdivi-1 interaction (Figure 3c) shows that 2-sulfanyl-4(3H)-quinazolinone spans a shallow cavity with its benzyl moiety facing the hydrophobic bottom formed by Val58, Gln34, and Gly133. Further, visual analysis portrays a strong H-bond interaction between the carboxyl group of Gly56 and the NH group at the 2-position of the quinazolinone moiety.

Validation of Docking by MD Simulation. Many hidden biological functions of proteins and their profound dynamic mechanisms can be revealed by studying their internal motions.³⁹ Likewise, to accurately identify the ligand-binding pocket and to really understand the interaction of a protein receptor with its ligand, we should consider not only the static structures concerned but also the dynamical information obtained by simulating their internal motions or dynamic process.⁴⁰

MD results were analyzed using tools bundled with the GROMACS distribution package. We selected the representative structure of each system to compare the protein structures, which was the closest conformation to the average structure during the last 10 ns of simulation. The root-mean-square deviation (RMSD) of backbone atoms of the protein revealed that Apo-form and Site-2 systems were slightly unstable during the initial phase of the simulation time i.e., up to 5000 ps. In the course of the second phase (5000–10000 ps), the RMSD values for Apo-form and Site-2 systems were sustained at an average value of 0.41 and 0.32 nm, respectively. Site-4 and Site-7 systems were mostly unstable with an average RMSD value of

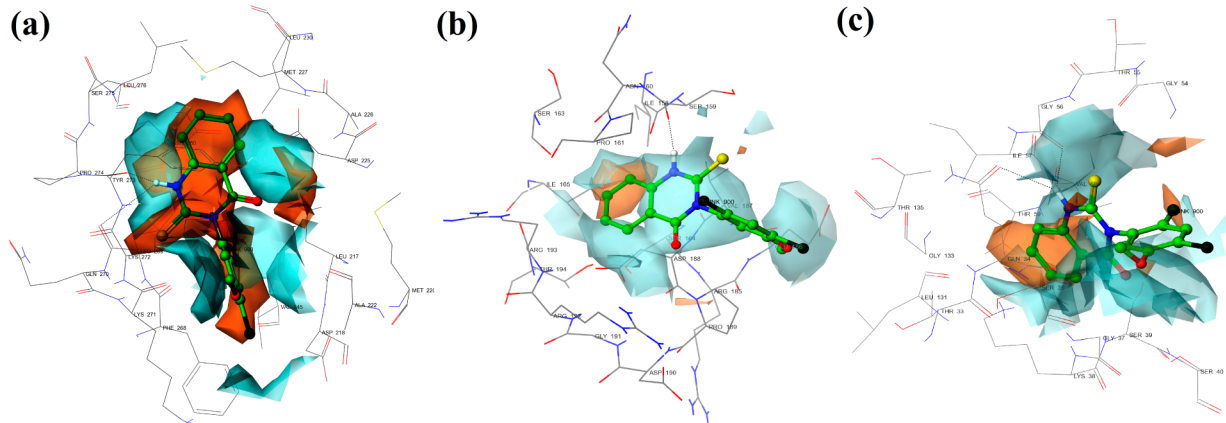


Figure 3. Binding poses obtained for the “most favorable sites”. For clarity, only interacting residues have been displayed. Black dotted lines represent H-bonds.

0.64 and 0.76 nm, respectively. The RMSD value for Site-2 was slightly lower than others. These fluctuations in RMSD conclude that the conformational flexibility of Drp1 seems to increase after the binding of inhibitor.

The total energy values of all the systems have shown smooth decreases until 2500 ps, and later they stabilized around a constant value (Supplementary 3), which explained that all the bound systems evolved with very similar system energies. Further, the MD-trajectory analysis of combined simulation depicts that Mdivi-1 fails to bind to the protein except at Site-2 (Supplementary 4). Visual analysis of the simulation trajectory revealed that after the contact, Mdivi-1 seems to induce pocket modification to the receptor, thus adapting to the cavity. During individual simulation, Mdivi-1 bound to the site-4 and site-7, but the contacts were superficial (Supplementary 5). According to the validation data, the Mdivi-1 tends to interact with the Drp1 at position Site-2. Hence, among the identified 8 receptors, the Site-2 receptor may represent most the probable binding site involved in the allosteric controlling of Drp1.

Mutational Analysis by MD Simulation. To determine the key amino acid residues in Site-2 that may be responsible for the Drp1 interaction with Mdivi-1, we replaced the “key residues” with other amino acids having with different sizes and charges.⁴¹ This study is likely to throw more light on the electrostatic nature of the Drp1 in terms of its canonical conformation and the canonical interactions with Mdivi-1. We replaced the amino acid residues viz., Leu217, Phe268, and Tyr273 identified during the docking study at the Site-2. MD results were analyzed using tools bundled with the GROMACS distribution package. The backbone root-mean-square deviation (RMSD) values of residues forming the binding site of the protein complex (Native Drp1-Mdivi1 and Mutant Drp1-Mdivi1) during 20 ns of MD simulations were calculated (Figure 4). The inhibitor mutant protein complex exhibited reasonable discrepancies in their RMSD values when compared to the native complex. Hence, it can be deduced that the Mdivi-1 was not stable on the mutant protein when compared to the native protein. We have also evaluated for the existing H-bond interactions between the ligand and the residues of Site-2, but there were no observable H-bond interactions between mutant and Mdivi-1. Further, the MD-trajectory visual analysis of simulation depicted that though the Mdivi-1 bound to the Site-2 cavity of the mutant, it was restricted to the rim of the cavity.

Structure Based Pharmacophore and Virtual Screening. The E-pharmacophore is a unique strategy that blends the

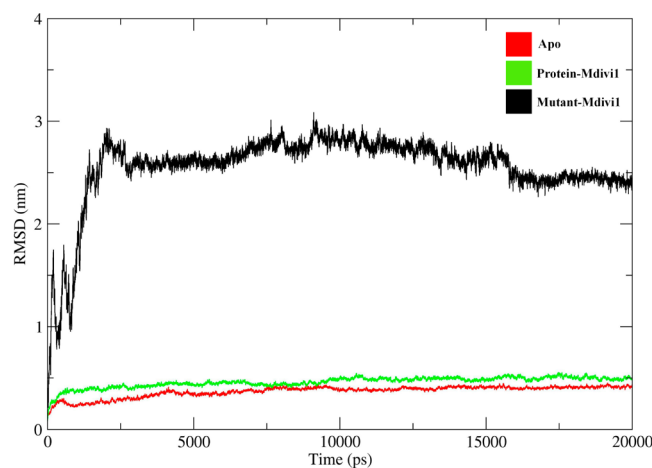


Figure 4. Comparison of root-mean-square deviation (RMSD) values of backbone atoms for the native and mutant Drp1.

beneficial aspects of structure-based and ligand-based techniques. Mounting evidence indicates the distinct advantage of incorporating protein–ligand interactions over the conventional ligand information alone for the analysis.^{42,43} The pharmacophore model was generated employing the energy descriptors obtained by fragment based probing of the Site-2. Based on these descriptors, a pharmacophore “fingerprint” was created from the Drp1 binding site. The selected 3D pharmacophore hypothesis (Figure 5) encompassed the following features: one H-bond acceptors [(A) (pink sphere with two arrows)], single H-bond donor [(D) (pale blue sphere with single arrow)], two hydrophobic groups [(H) (green sphere)], and three aromatic ring features [(R) (orange ring)]. Further, the atomic coordinates of the ADHHRRR were used to screen the ZINC database using ZincPharmer server to retrieve potential compounds having these pharmacophoric features. Altogether, 1357 matches were fetched out of 13 million structures.

Docking Mode Analysis. To further refine the retrieved hits, 1357 hits were docked into the Site-2 of Drp1. The binding modes for 1357 compounds identified by docking were ranked according to G-score values. The 50 highest scoring compounds were selected for further evaluation. After visual inspection, the most favorable compounds with the best binding modes and structural diversity were selected. Based on

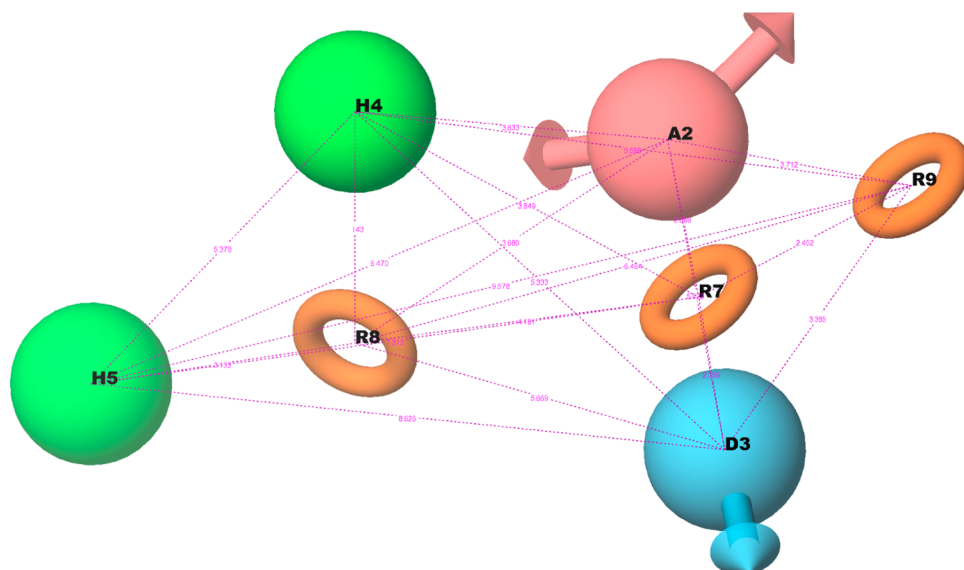


Figure 5. Pharmacophore model with intersite distances. Hypothesis consists of one H-bond acceptor (A), one H-bond donor (D), two hydrophobic features (H), and three aromatic ring features (R). Pink spheres with vectors represent an acceptor feature, blue spheres with vectors represent a donor feature, an orange ring represents an aromatic feature, and a green sphere symbolizes a hydrophobic group.

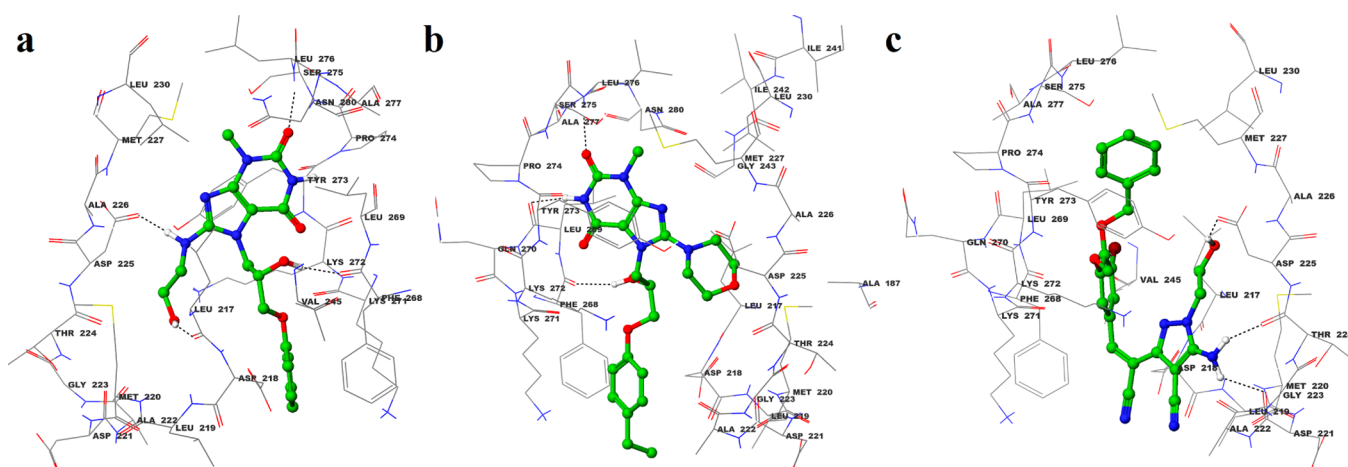


Figure 6. “Top scored hits” docked into the Site-2 of Drp1. For clarity, only interacting residues have been displayed. Black dotted lines represent H-bonds

the knowledge of the existing Drp1 inhibitors, we selected 3 compounds out of 50 highest scoring structures. The structures of these best hits from the final screening are reported in Figure 6

Neuroprotective Studies *in Vivo*. The nematode round-worm, *Caenorhabditis elegans*, is ideal for neurodegenerative disease studies. It is genetically amenable, has a short life span, and a well-defined nervous system. Fluorescent markers, like GFP, are readily visualized in *C. elegans* as it is a transparent organism; thus the nervous system, and the factors that alter the viability of neurons, can be directly examined *in vivo*. Through expression of the human disease protein α -synuclein in the worm's dopamine neurons, neurodegeneration is observed in an age-dependent manner.⁴⁴ Described herein are techniques employed with *C. elegans* to evaluate the neuro-protective efficacy of candidate Drp1 inhibitors against α -synuclein induced neurodegeneration.

The DRP-1 gene in *C. elegans* is a very close relative of human Drp1. The DRP-1 cDNAs encode a 79 kDa protein

with the characteristic arrangement of protein domains found in other dynamin family members.⁴⁵ Overall, the sequence of human Drp1 is most closely related to a *Caenorhabditis elegans* dynamin-related protein (62% amino acid identity, GTPase domain represents 71% identity).⁴⁶ Furthermore, inhibition of Drp1 in *C. elegans* prevented the fragmentation and apoptosis, suggesting that the mitochondrial participation in apoptosis seems to be conserved from worms to mammals. Therefore, it can be deduced that the DRP-1 proteins from these species are functional homologues.

Locomotory Rate and Pharyngeal Pumping Assays.

Locomotion in *C. elegans* is achieved by a reciprocal contraction and relaxation of the dorsal and ventral body-wall muscles, producing a sinusoidal wave of movement. This sinusoidal wave propagates along the length of the worm body, generating a body bend, which propels the worm forward or backward.

A complex neuronal network involving fast transmitter release mechanisms is known to regulate this locomotory system. *C. elegans* produces a characteristic thrashing movement

when placed in liquid, and this behavior can be used to quantify locomotion defects because, unlike worm movement on a solid substrate, thrashing is both continuous and high frequency. In the present study, analysis of the thrashing behavior indicated that the body bends in worms was significantly low in untreated UA44 control group. However, the drug treated worms demonstrated statistically significant increase ($p < 0.05$) in thrashing behavior comparable to wildtype (N2) animals (Figure 7).

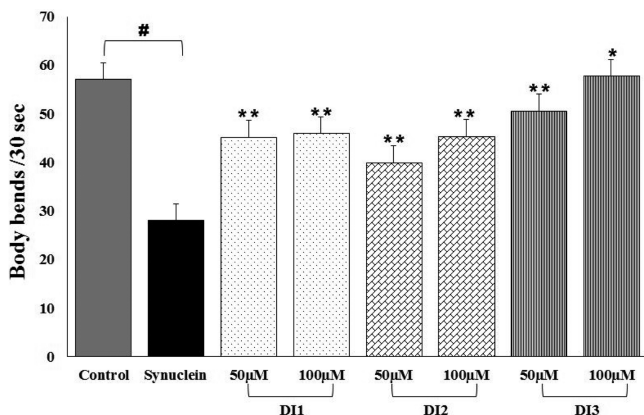


Figure 7. Locomotory rate (frequency of bending) of wildtype (N2) animals, drug untreated animals (α -synuclein overexpression strain), Drp1inhibitor-treated (α -synuclein overexpression strain). The data represent the mean \pm SE ($n = 10$). A hash (#) indicates significant differences between wildtype (N2) and untreated animals ($p < 0.01$); an asterisk (*) indicates significant differences between the wildtype (N2) samples and the Drp1 inhibitor-treated samples (* $p < 0.05$, ** $p < 0.01$).

The neuromuscular pharynx allows the worm to ingest the bacteria. Rhythmic contraction and relaxation of this organ transports food from the mouth to the intestine. The pumping rate progressively declines during synuclein mediated neurodegeneration. Numerous studies have demonstrated that pharyngeal pumping rates can be pharmacologically modulated.^{47,48} In the present study, administration of Drp1 inhibitors positively modulated the pharyngeal pumping rates by blocking DA neurodegeneration. Wildtype (N2) worms defined as the control for our pharyngeal pumping studies displayed 62 ± 5 pharyngeal pumps per 20 s. The pharyngeal pumping rate (28 ± 5 per 20 s) declined significantly in the case of the untreated UA44 (α -synuclein) strain. However, the worms treated with Drp1 inhibitors exhibited significant recovery in pharyngeal pumping (58 ± 5 per 20 s) (Figure 8).

C. elegans Neurodegeneration Assay. To evaluate the role of DI1, 2, and 3 in protection against dopamine (DA) neuron loss in *C. elegans*, we employed two transgenic *C. elegans* model of viz., Pdat-1::GFP animals (BZ555) and Pdat-1:: α -syn (UA44) α -syn-induced neurodegeneration strain. Since the nematode is transparent and its development is tightly regulated, it allows for rapid quantitative assessment of morphological changes in the six anterior DA neurons.

The expression of α -synuclein and GFP under the control of DA transporter promoter (Pdat-1) resulted in an age-dependent degeneration of DA neurons, whereby 83 and 90% loss of neurons at 10 days. We were curious to determine whether the treatment of DI1, 2, and 3, would reduce the amount of DA neurodegeneration. Accordingly, treatment with

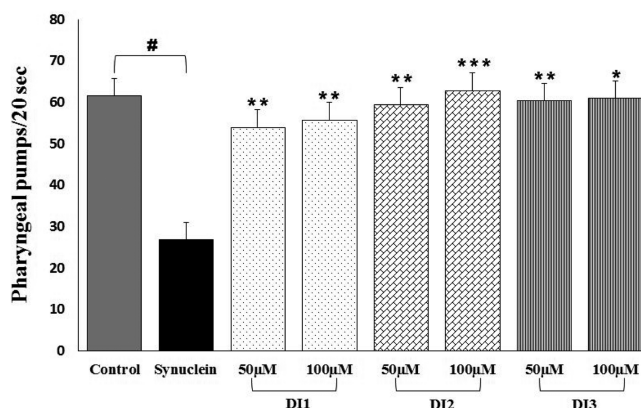


Figure 8. Pharyngeal pumping rate (frequency of pharyngeal movement) of wildtype (N2) animals, drug untreated animals (α -synuclein overexpression strain), Drp1inhibitor-treated (α -synuclein overexpression strain). The data represent the mean \pm SE ($n = 10$). A hash (#) indicates significant differences between wildtype (N2) and untreated animals ($p < 0.01$); an asterisk (*) indicates significant differences between the wildtype (N2) samples and the Drp1 inhibitor-treated samples (* $p < 0.05$, ** $p < 0.01$, *** $p < 0.001$).

100 μ M concentration of Drp1 inhibitors significantly abolished the DA neuronal degeneration in the drug treated animals (Figure 9).

CONCLUSIONS

The present study depicts a novel approach to identify cryptic binding sites to utilize in drug discovery processes. To the best of our knowledge, this is the first study to delineate molecular interactions responsible for the binding of Mdivi-1 to the Drp1. 3D structure of the Drp1 was developed using custom-based homology modeling protocol. The surface of the Drp1 structure was scrutinized for probable binding sites. An array of putative binding sites was subsequently subjected to docking based screening by employing Mdivi-1. The docking mode analysis yielded three potential sites, which were later subjected to the validation by MD simulations. The MD simulation process fetched Site-2 as the most probable binding site. Site-2 demonstrated the better interaction profile with Mdivi-1 and could be a possible region of Drp1 binding. The predicted cryptic binding Site- 2 was further employed in inhibitor prediction process. In this approach, a highly efficient pharmacophore hypothesis was developed consisting seven point features (ADHRRR). Pharmacophore-based database searching was considered followed by docking-based VS. Finally, the docking based screening fetched 50 hit structures of which 3 highest scoring compounds were evaluated for their neuroprotective efficacy in *C. elegans* model of Parkinson's disease. We employed UA44 transgenic α -synuclein strains and evaluated the antiparkinsonian effects of Drp1 inhibitors. As shown in Figure 7 and 8, the Drp1 inhibitors significantly restored the behavioral deficits in the α -syn/UA44 transgenic worms. Further, the exogenous treatment of α -syn/UA44 worms with Drp1 inhibitors rescued the dopaminergic loss. The new lead compounds displayed significant antiparkinsonian effects and potently inhibited the degeneration of DA neurons. Our findings on the neuroprotective potential of Drp1-selective inhibitors should encourage further validation in preclinical and clinical settings.

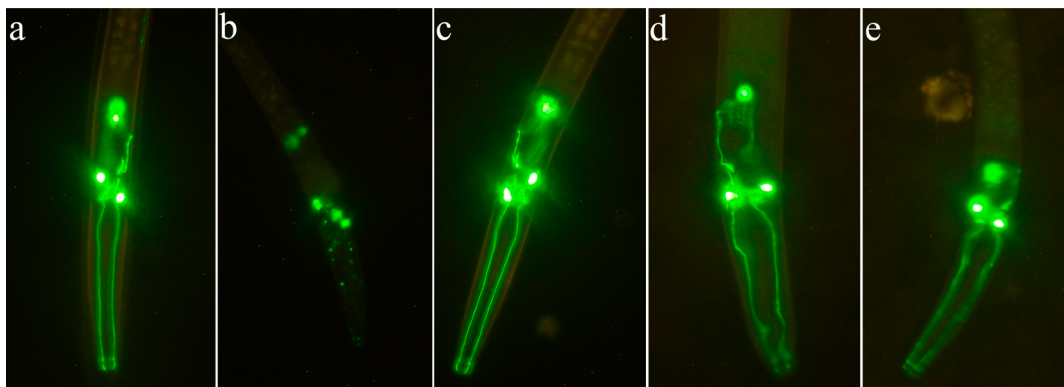


Figure 9. α -Synuclein expression leads to DA neurodegeneration. (a) *C. elegans* expressing GFP marker with intact DA neurons, (b) *C. elegans* α -synuclein overexpression strains displayed prominent loss of DA neurons and broken neuritis during adulthood, and (c), (d), and (e) Drp1 inhibitors ($100 \mu\text{M}$) markedly protected the DA neurons from α -synuclein induced neurodegenerartion.

ASSOCIATED CONTENT

Supporting Information

Video data files of the Molecular dynamic simulations. This material is available free of charge via the Internet at <http://pubs.acs.org>.

AUTHOR INFORMATION

Corresponding Author

*Phone: 91 495 228 5452. Fax: +91 495 228 7250. E-mail: rajanikant@nitc.ac.in. Corresponding author address: DBT - Center for Bioinformatics, National Institute of Technology Calicut, Calicut 673601, India.

Notes

Disclosure: The authors report no declarations of interest. The authors declare no competing financial interest.

REFERENCES

- (1) Wu, D. C.; Jackson-Lewis, V.; Vila, M.; Tieu, K.; Teismann, P.; Vadseth, C.; Choi, D. K.; Ischiropoulos, H.; Przedborski, S. Blockade of microglial activation is neuroprotective in the 1-methyl-4-phenyl-1,2,3,6-tetrahydropyridine mouse model of Parkinson disease. *J. Neurosci.* **2002**, *22*, 1763–71.
- (2) Winklhofer, K. F.; Haass, C. Mitochondrial dysfunction in Parkinson's disease. *Biochim. Biophys. Acta* **2010**, *1802*, 29–44.
- (3) Burbulla, L. F.; Krebsiehl, G.; Krüger, R. Balance is the challenge—the impact of mitochondrial dynamics in Parkinson's disease. *Eur. J. Clin. Invest.* **2010**, *40*, 1048–1060.
- (4) Gomez-Lazaro, M.; Bonekamp, N. A.; Galindo, M. F.; Jordán, J.; Schrader, M. 6-Hydroxydopamine (6-OHDA) induces Drp1-dependent mitochondrial fragmentation in SH-SY5Y cells. *Free Radical Biol. Med.* **2008**, *44*, 1960–1969.
- (5) Lim, K. L.; Ng, X. H.; Grace, L. G.; Yao, T. P. Mitochondrial dynamics and Parkinson's disease: focus on parkin. *Antioxid. Redox Signaling* **2012**, *16*, 935–949.
- (6) Song, W.; Chen, J.; Petrilli, A.; Liot, G.; Klinglmayr, E.; Zhou, Y.; Poquiz, P.; Tjong, J.; Pouladi, M. A.; Hayden, M. R.; Masliah, E.; Ellisman, M.; Rouiller, I.; Schwarzenbacher, R.; Bossy, B.; Perkins, G.; Bossy-Wetzel, E. Mutant huntingtin binds the mitochondrial fission GTPase dynamin-related protein-1 and increases its enzymatic activity. *Nat. Med.* **2011**, *17*, 377–382.
- (7) Esteves, A. R.; Arduíño, D. M.; Silva, D. F.; Oliveira, C. R.; Cardoso, S. M. Mitochondrial Dysfunction: The Road to Alpha-Synuclein Oligomerization in PD. *Parkinson's Dis.* **2011**, *2011*, 693761.
- (8) Gao, D.; Zhang, L.; Dhillon, R.; Hong, T. T.; Shaw, R. M.; Zhu, J. Dynasore protects mitochondria and improves cardiac lusitropy in Langendorff perfused mouse heart. *PLoS One* **2013**, *8*, e60967–e60975.
- (9) Qi, X.; Qvit, N.; Su, Y. C.; Mochly-Rosen, D. A novel Drp1 inhibitor diminishes aberrant mitochondrial fission and neurotoxicity. *J. Cell Sci.* **2013**, *126*, 789–802.
- (10) Park, S. W.; Kim, K. Y.; Lindsey, J. D.; Dai, Y.; Heo, H.; Nguyen, D. H.; Ellisman, M. H.; Weinreb, R. N.; Ju, W. K. A selective inhibitor of drp1, mdivi-1, increases retinal ganglion cell survival in acute ischemic mouse retina. *Invest. Ophthalmol. Visual Sci.* **2011**, *52*, 2837–2843.
- (11) Zhang, N.; Wang, S.; Li, Y.; Che, L.; Zhao, Q. A selective inhibitor of Drp1, mdivi-1, acts against cerebral ischemia/reperfusion injury via an anti-apoptotic pathway in rats. *Neurosci. Lett.* **2013**, *535*, 104–109.
- (12) Hardy, J. A.; Wells, J. A. Searching for new allosteric sites in enzymes. *Curr. Opin. Struct. Biol.* **2004**, *14*, 706–715.
- (13) Niemann, H. H.; Knetsch, M. L.; Scherer, A.; Manstein, D. J.; Kull, F. J. Crystal structure of a dynamin GTPase domain in both nucleotide-free and GDP-bound forms. *EMBO J.* **2001**, *20*, 5813–5821.
- (14) Hanumanthappa, P.; Rajanikant, G. K. In silico identification of potential dynamin-related protein 1 antagonists: implications for diseases involving mitochondrial dysfunction. *Comb. Chem. High Throughput Screening* **2014**, *17*, 25–34.
- (15) Pradeep, H.; Sharma, B.; Rajanikant, G. K. Drp1 in ischemic neuronal death: An unusual suspect. *Curr. Med. Chem.* **2014**, *21*, 2183–2189.
- (16) Davis, I. W.; Murray, L. W.; Richardson, J. S.; Richardson, D. C. MOLPROBITY: structure validation and all-atom contact analysis for nucleic acids and their complexes. *Nucleic Acids Res.* **2004**, *32*, W615–W619.
- (17) Laskowski, R. A.; MacArthur, M. W.; Moss, D. S.; Thornton, J. M. PROCHECK: a program to check the stereochemical quality of protein structures. *J. Appl. Crystallogr.* **1993**, *26*, 283–291.
- (18) Halgren, T. A. Identifying and characterizing binding sites and assessing druggability. *J. Chem. Inf. Model.* **2009**, *49*, 377–389.
- (19) Teli, M. K.; Pradeep, H.; Rajanikant, G. K. Pharmacophore generation and 3D-QSAR of novel 2-(quinazolin-4-ylamino)-[1,4]benzoquinone derivatives as VEGFR-2 inhibitors. *Lett. Drug Des. Discovery* **2012**, *9*, 899–914.
- (20) Nair, S. B.; Fayaz, S. M.; Krishnamurthy, R. G. In silico prediction of novel inhibitors of the DNA binding activity of FoxG1. *Med. Chem.* **2012**, *8*, 1155–1162.
- (21) Nair, S. B.; Teli, M. K.; Pradeep, H.; Rajanikant, G. K. Computational identification of novel histone deacetylase inhibitors by docking based QSAR. *Comput. Biol. Med.* **2012**, *42*, 697–705.
- (22) Teli, M. K.; Rajanikant, G. K. Identification of novel potential HIF-prolyl hydroxylase inhibitors by in silico screening. *Mol. Diversity* **2012**, *16*, 193–202.
- (23) Hanumanthappa, P.; Teli, M. K.; Krishnamurthy, R. G. Generation of pharmacophore and atom based 3D-QSAR model of

- novel isoquinolin-1-one and quinazolin-4-one-type inhibitors of TNF α . *Med. Chem.* **2012**, *8*, 436–451.
- (24) Teli, M. K.; Rajanikant, G. K. A Combination of 3D-QSAR modeling and molecular docking approach for the discovery of potential HIF Prolyl Hydroxylase inhibitors. *Med. Chem.* **2012**, *9*, 360–370.
- (25) Halgren, T. A.; Murphy, R. B.; Friesner, R. A.; Beard, H. S.; Frye, L. L.; Pollard, W. T.; Banks, J. L. Glide: a new approach for rapid, accurate docking and scoring. 2. Enrichment factors in database screening. *J. Med. Chem.* **2004**, *47*, 1750–1759.
- (26) Friesner, R. A.; Banks, J. L.; Murphy, R. B.; Halgren, T. A.; Klicic, J. J.; Mainz, D. T.; Repasky, M. P.; Knoll, E. H.; Shelley, M.; Perry, J. K.; Shaw, D. E.; Francis, P.; Shenkin, P. S. Glide: a new approach for rapid, accurate docking and scoring. 1. Method and assessment of docking accuracy. *J. Med. Chem.* **2004**, *47*, 1739–1749.
- (27) Hess, B.; Kutzner, C.; van der Spoel, D.; Lindahl, E. GROMACS 4: Algorithms for Highly Efficient, Load-Balanced, and Scalable Molecular Simulation. *J. Chem. Theory Comput.* **2008**, *4*, 435–447.
- (28) Oostenbrink, C.; Villa, A.; Mark, A. E.; van Gunsteren, W. F. A biomolecular force field based on the free enthalpy of hydration and solvation: the GROMOS force-field parameter sets 53A5 and 53A6. *J. Comput. Chem.* **2004**, *25*, 1656–1676.
- (29) Schüttelkopf, A. W.; van Aalten, D. M. PRODRG: a tool for high-throughput crystallography of protein-ligand complexes. *Acta Crystallogr., Sect. D: Biol. Crystallogr.* **2004**, *60*, 1355–1363.
- (30) Jorgensen, W. L.; Chandrasekhar, J.; Madura, J. D.; Impey, R. W.; Klein, M. L. Comparison of simple potential functions for simulating liquid water. *J. Chem. Phys.* **1983**, *79*, 926–935.
- (31) Berendsen, H. J. C.; Postma, J. P. M.; Van Gunsteren, W. F.; DiNola, A.; Haak, J. R. Molecular dynamics with coupling to an external bath. *J. Chem. Phys.* **1984**, *81*, 3684–3691.
- (32) Darden, T.; York, D.; Pedersen, L. Particle mesh ewald – an N. log(N) method for ewald sums in large systems. *J. Chem. Phys.* **1993**, *98*, 10089–10093.
- (33) Humphrey, W.; Dalke, A.; Schulten, K. VMD: visual molecular dynamics. *J. Mol. Graphics* **1996**, *14*, 33–38.
- (34) Pradeep, H.; Rajanikant, G. K. A rational approach to selective pharmacophore designing: an innovative strategy for specific recognition of Gsk3 β . *Mol. Diversity* **2012**, *16*, 553–562.
- (35) Koes, D. R.; Camacho, C. J. ZINCPharmer: pharmacophore search of the ZINC database. *Nucleic Acids Res.* **2012**, *40*, W409–W414.
- (36) Harrington, A. J.; Knight, A. L.; Caldwell, G. A.; Caldwell, K. A. Caenorhabditis elegans as a model system for identifying effectors of α -synuclein misfolding and dopaminergic cell death associated with Parkinson's disease. *Methods* **2011**, *53*, 220–225.
- (37) Brenner, S. The genetics of Caenorhabditis elegans. *Genetics* **1974**, *77*, 71–94.
- (38) Jones, A. K.; Rayes, D.; Al-Diwani, A.; Maynard, T. P.; Jones, R.; Hernando, G.; Buckingham, S. D.; Bouzat, C.; Sattelle, D. B. A Cys-loop mutation in the Caenorhabditis elegans nicotinic receptor subunit UNC-63 impairs but does not abolish channel function. *J. Biol. Chem.* **2011**, *286*, 2550–2558.
- (39) Frecer, V. Theoretical prediction of drug-receptor interactions. *Drug Metab. Drug Interact.* **2011**, *26*, 91–104.
- (40) Dror, R. O.; Dirks, R. M.; Grossman, J. P.; Xu, H.; Shaw, D. E. Biomolecular simulation: a computational microscope for molecular biology. *Annu. Rev. Biophys.* **2012**, *41*, 429–452.
- (41) Dasgupta, J.; Sen, U.; Dattagupta, J. K. In silico mutations and molecular dynamics studies on a winged bean chymotrypsin inhibitor protein. *Protein Eng.* **2003**, *16*, 489–496.
- (42) Tan, L.; Lounkine, E.; Bajorath, J. Similarity searching using fingerprints of molecular fragments involved in protein-ligand interactions. *J. Chem. Inf. Model.* **2008**, *48*, 2308–2312.
- (43) Ballester, P. J.; Mitchell, J. B. A machine learning approach to predicting protein-ligand binding affinity with applications to molecular docking. *Bioinformatics* **2010**, *26*, 1169–1175.
- (44) Tucci, M.; Harrington, A. J.; Caldwell, G. A.; Caldwell, K. A. Modeling dopamine neuron degeneration in *Caenorhabditis elegans*. *Methods. Mol. Biol.* **2011**, *793*, 129–148.
- (45) Labrousse, A. M.; Zappaterra, M. D.; Rube, D. A.; van der Bliek, A. M. *C. elegans* dynamin-related protein DRP-1 controls severing of the mitochondrial outer membrane. *Mol. Cell* **1999**, *4*, 815–826.
- (46) Smirnova, E.; Shurland, D. L.; Ryazantsev, S. N.; van der Bliek, A. M. A human dynamin-related protein controls the distribution of mitochondria. *J. Cell. Biol.* **1998**, *143*, 351–358.
- (47) Lemieux, G. A.; Keiser, M. J.; Sassano, M. F.; Laggner, C.; Mayer, F.; Bainton, R. J.; Werb, Z.; Roth, B. L.; Shoichet, B. K.; Ashrafi, K. In silico molecular comparisons of *C. elegans* and mammalian pharmacology identify distinct targets that regulate feeding. *PLoS Biol.* **2013**, *11*, e1001712–e1001719.
- (48) Dimitriadi, M.; Kye, M. J.; Kalloo, G.; Yersak, J. M.; Sahin, M.; Hart, A. C. The neuroprotective drug riluzole acts via small conductance Ca^{2+} -activated K^+ channels to ameliorate defects in spinal muscular atrophy models. *J. Neurosci.* **2013**, *33*, 6557–6562.